

Dalton Transactions

Accepted Manuscript



This is an *Accepted Manuscript*, which has been through the Royal Society of Chemistry peer review process and has been accepted for publication.

Accepted Manuscripts are published online shortly after acceptance, before technical editing, formatting and proof reading. Using this free service, authors can make their results available to the community, in citable form, before we publish the edited article. We will replace this *Accepted Manuscript* with the edited and formatted *Advance Article* as soon as it is available.

You can find more information about *Accepted Manuscripts* in the [Information for Authors](#).

Please note that technical editing may introduce minor changes to the text and/or graphics, which may alter content. The journal's standard [Terms & Conditions](#) and the [Ethical guidelines](#) still apply. In no event shall the Royal Society of Chemistry be held responsible for any errors or omissions in this *Accepted Manuscript* or any consequences arising from the use of any information it contains.

Cite this: DOI: 10.1039/c0xx00000x

www.rsc.org/xxxxxx

ARTICLE TYPE

Magnetic and magnetocaloric properties of an unusual family of carbonate-panelled [Ln^{III}₆Zn^{II}₂] cages

Waqas Sethi,^{a,b} Sergio Sanz,^b Kasper S. Pedersen,^a Mikkel A. Sørensen,^a Gary S. Nichol,^b Giulia Lorusso,^c Marco Evangelisti,^{*c} Euan K. Brechin^{*a} and Stergios Piligkos^{*a}

Received (in XXX, XXX) Xth XXXXXXXXX 20XX, Accepted Xth XXXXXXXXX 20XX

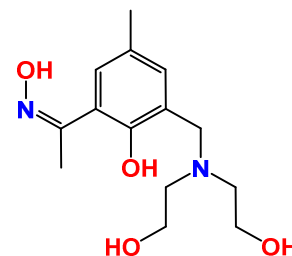
DOI: 10.1039/b000000x

The reaction of the pro-ligand H₄L, which combines the complementary phenolic oxime and diethanolamine moieties within the same organic framework, with Zn(NO₃)₂·6H₂O and Ln(NO₃)₃·6H₂O in a basic methanolic solution generates a family of isostructural heterometallic coordination compounds of general formula [Ln₆Zn₂(CO₃)₅(OH)(H₂L)₄(H₃L)₂(H₄L)]NO₃·xMeOH [Ln = Gd, x = 30 (1), Ln = Dy, x = 32 (2), Ln = Sm, x = 31 (3), Ln = Eu, x = 29 (4), Ln = Tb, x = 30 (5)]. The octametalllic skeleton of the cage describes a heavily distorted [Gd^{III}₆] octahedron capped on two faces by Zn^{II} ions. The metal core is stabilised by a series of μ₃- and μ₄-CO₃²⁻ ions, originating from the serendipitous fixation of atmospheric CO₂. The magnetic properties of all family members were examined *via* SQUID magnetometry, with the χ_MT product and VTVB data of the Gd analogue (1) being independently fitted by numerical diagonalisation to afford the same best-fit parameter J_{Gd-Gd} = -0.004 cm⁻¹. The MCE of complex 1 was elucidated from specific heat data, with the magnetic entropy change reaching a value of 22.6 J kg⁻¹ K⁻¹ at T = 1.7 K, close to the maximum entropy value per mole expected from six Gd^{III} spins (S_{Gd} = 7/2), 23.7 J kg⁻¹ K⁻¹.

Introduction

The large value of their total angular momentum, their often strong magnetic anisotropy and the inherently weak magnetic exchange mediated *via* their contracted *f*-orbitals engender Ln-based molecular cages with some fascinating and potentially useful low temperature physics.¹⁻⁵ In academia these have been much exploited for the construction of Single-Molecule Magnets (SMMs)⁶ and Molecular Coolers.⁷ The prospect of employing molecular cages in low temperature cooling applications is based upon the compounds magneto-caloric effect (MCE), as derived from the change in magnetic entropy upon application of a magnetic field.⁸ The design of such molecular materials therefore requires the control and optimisation of quantum properties at the molecular level (spin ground state, magnetic anisotropy, the presence of low-lying excited spin states), which in turn requires the synthetic chemist to follow a particular recipe that includes high spin, anisotropic metal ions and lightweight organic bridging ligands.⁹

When a magnetic field is applied to a polynuclear molecular magnetic material in which the magnetic exchange interaction between constitutive metal centres and the local magnetic anisotropies are small, the magnetic moments of the constitutive paramagnetic centres become polarised by the magnetic field. When this magnetisation process is performed at constant temperature, the total magnetic entropy of the material is reduced. In a subsequent adiabatic demagnetisation process, the temperature of the material decreases, thereby cooling the material.¹⁰ This is a particularly attractive, and potentially



Scheme 1. The structure of the ligand H₄L which contains both phenolic oxime and diethanolamine moieties.

technologically important phenomenon, since recent studies have shown that the MCE of some molecular clusters can be much larger than that found in the best intermetallic and lanthanide alloys, and magnetic nanoparticles employed commercially.¹¹⁻¹² The obvious metal ion of choice is Gd^{III} since it possesses an isotropic *S* = 7/2, and its clusters will exhibit weak magnetic exchange courtesy of the contracted *f*-orbitals, resulting in the presence of field-accessible, low-lying excited states. Indeed the vast majority of clusters reported recently to display an enhanced MCE have contained multiple Gd^{III} centres.¹³⁻¹⁸ We continue this trend by reporting the syntheses, structures, magnetic and magnetocaloric properties of a rather unusual set of complexes of general formula [Ln₆Zn₂(CO₃)₅(OH)(H₂L)₄(H₃L)₂(H₄L)₅]NO₃·x MeOH [Ln = Gd, x = 30 (1), Ln = Dy, x = 32 (2), Ln = Sm, x = 31 (3), Ln = Eu, x = 29 (4), Ln = Tb, x = 30 (5)] built with the ligand (*Z*)-1-(3-(bis(2-hydroxyethyl)amino)methyl)-2-hydroxy-5-methylphenyl)ethan-1-one oxime, [H₄L], shown in Scheme 1.

We have previously shown that this ligand is highly effective in forming transition metal cages with aesthetically pleasing structures and fascinating magnetic properties, and we now extend its coordination chemistry to the $4f$ elements.¹⁹

5 Experimental

Materials and physical measurements

All manipulations were performed under aerobic conditions, using materials as received (reagent grade). (Z)-1-(3-((bis(2-hydroxyethyl)amino)methyl)-2-hydroxy-5-methylphenyl)ethan-1-one oxime) [H_4L] was synthesised as described in the literature.¹⁹ Magnetisation data were acquired on a MPMS-XL SQUID magnetometer equipped with a 5 T dc magnet. Freshly isolated crystalline material was covered immediately with hexadecane (MPt = 18 °C) in order to suppress loss of co-crystallized solvent. Dc susceptibility data were obtained with $H_{dc} = 1000$ Oe in the temperature range 1.8–280 K and magnetisation data at $H_{dc} \leq 50$ kOe at selected low temperatures. All data were corrected for diamagnetic contributions from the sample, hexadecane and the capsule by means of Pascals constants. Specific heat measurements were carried out at temperatures down to 0.3 K by using a Quantum Design 9T-PPMS, equipped with a ^3He cryostat. The experiments were performed on thin pressed pellets (*ca.* 1 mg) of a polycrystalline sample, thermalised by *ca.* 0.2 mg of Apiezon N grease, whose contribution was subtracted using a phenomenological expression.

Syntheses

General synthetic procedure for complexes **1-3**: $\text{Ln}(\text{NO}_3)_3 \cdot x\text{H}_2\text{O}$ (0.25 mmol), $\text{Zn}(\text{NO}_3)_2 \cdot 6\text{H}_2\text{O}$ (75 mg, 0.25 mmol), H_4L (140 mg, 0.5 mmol), $^i\text{BuONa}$ (100 mg, 1 mmol) and Et_3N (300 μL , 2.15 mmol) were stirred in 25 ml MeOH for 2 hours. The solution was then filtered and allowed to stand. X-ray quality crystals formed *via* slow evaporation of the mother liquor over a period of 5 days in ~30–40 % yield. Complex **4** was made in the same manner, but using 0.5 mmol (100mg) $^i\text{BuONa}$, whilst no $^i\text{BuONa}$ was added to the reaction mixture to make **5**. Elemental analyses, calculated (found): **1**: C 36.18 (36.24), H 4.27 (4.61), N 6.14 (6.19). **2**: C 35.85 (34.97), H 4.24 (4.52), N 6.09 (5.81). **3**: C 36.62 (35.40), H 4.33 (4.28), N 6.22 (5.92). **4**: C 36.52 (35.36), H 4.31 (4.38), N 6.20 (5.73). **5**: C 36.07 (34.91), H 4.26 (4.42), N 6.13 (5.95).

X-ray crystallography

Diffraction data were collected on a Bruker Smart Apex CCD diffractometer equipped with an Oxford Cryosystems LT device, using Mo radiation. Data collection parameters and structure solution and refinement details are listed in Table S1. Full details can be found in the CIF files provided in the supporting information and CCDC 1055091-1055095.

Results and Discussion

Compounds **1-5** are isostructural, and so for the sake of brevity we limit discussion to complex **1**, [$\text{Gd}^{\text{III}}_6\text{Zn}^{\text{II}}_2(\text{CO}_3)_5(\text{OH})(\text{H}_2\text{L})_4(\text{H}_3\text{L})_2(\text{H}_4\text{L})$] $\text{NO}_3 \cdot 30\text{MeOH}$ (Figure 1). The metallic skeleton of the cage describes a highly distorted [Gd^{III}_6] octahedron with the two Zn^{II} ions each capping a triangular face. The core of the molecule is stabilised by the presence of five CO_3^{2-} ions, originating from the serendipitous fixation of

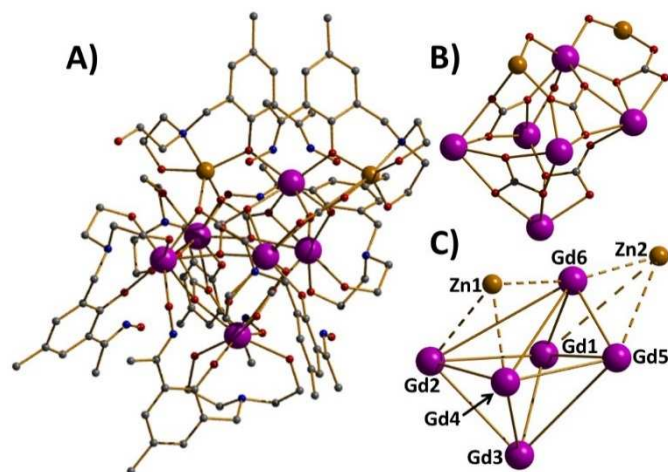
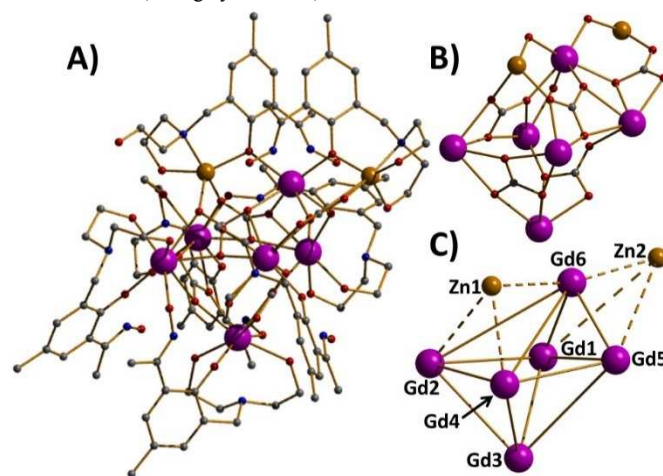
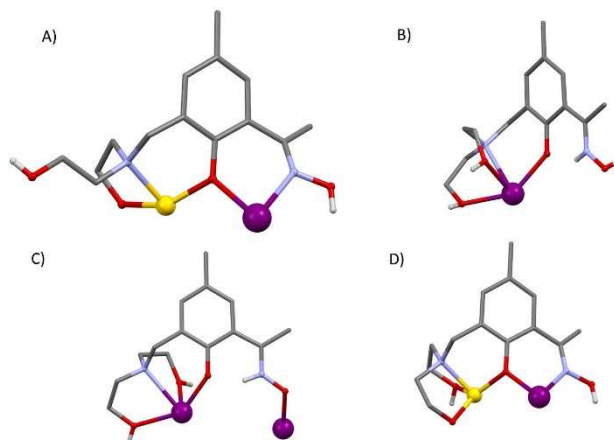


Figure 1. A) The structure of the cation of complex **1**. B) The metal core highlighting the role of the bridging carbonate ions. C) The metal skeleton of the cage emphasising the highly distorted Gd octahedron and two face-capping Zn ions. Colour code: Gd = purple, Zn = gold, O = red, N = blue, C = grey. H atoms, the nitrate counter ion and solvent



molecules of crystallisation are omitted for clarity.

atmospheric CO_2 . These exhibit several different bonding modes [$\mu_3\text{-Gd}_3$, $\mu_3\text{-Gd}_2\text{Zn}$, $\mu_3\text{-Gd}_4$, $\mu_4\text{-Gd}_4$, $\mu_4\text{-Gd}_2\text{Zn}_2$] as shown in Figure 1B. There is a single OH^- ion which μ -bridges between Gd_4 and Gd_6 (Gd-O-Gd , 112°) and four H_2L^{2-} , two H_3L^- and one H_4L ligands that adorn the outer periphery of the molecule. These



ligands exhibit four different coordination modes as shown in Figure 2: the majority bond in a μ -fashion along the edges of the

Gd octahedron, or between a Gd vertex and a Zn cap. One ligand (H₄L) chelates Gd³⁺ through its phenolic and alkoxide O-atoms, with its oximic O- and N-atoms remaining non-coordinating, and H-bonding to the alkoxide O-atom on a neighbouring ligand (O...O, ~2.6 Å). Indeed all of the organic ligands are involved in extensive intramolecular H-bonding interactions with their neighbouring ligands and to the MeOH molecules of crystallisation (Figure S2-3). All of the Gd ions are nine coordinate {GdO₈N} and in capped square antiprismatic geometries, with the exception of Gd₆ which is eight coordinate {GdO₆N₂} and square antiprismatic; the latter being the only Ln ion that is not chelated by the diethanolamine moieties. The Zn ions are both five coordinate {ZnO₄N} and in distorted trigonal bipyramidal geometries.

There are several close intermolecular contacts. The diethanolamine O-atoms coordinated to Zn₂ are H-bonding to the equivalent group on their nearest neighbour (O...O, 2.46 Å; Zn...Zn, 4.14 Å), and at the opposite end of the molecule the Ph rings of the organic ligands are involved in π ... π stacking interactions (C...C, 3.58 Å). The result is the formation of a serpentine-like H-bonded chain of cationic cages (Figure S3). Closest contacts between these chains are through the Me-groups on the Ph rings of the organic ligand and between the same moiety and the -CH₂ arms of the diethanolamine unit (Me...CH₃/CH₂, ~4 Å). This produces a 2D sheets of cations of **1** forming an overall layered structure in the crystal (Figure S3). The presence of the carbonate ligands is intriguing, and one that is becoming ever more prevalent with the increasing number of Ln-based cages being reported. Of the ~130 entries in the CSD of metal cluster compounds containing carbonate anions

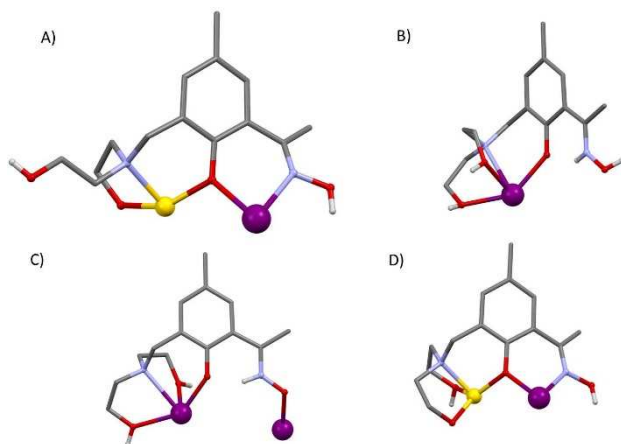


Figure 2. The different bonding modes of the H₂L²⁻, H₃L⁻ and H₄L ligands highlighting the diverse levels of protonation.

approximately ~25% are 4f complexes and ~5% are heterometallic 3d-4f complexes.²⁰ While the majority have been formed serendipitously, this observation has led some researchers to deliberately employ Na₂CO₃, NaHCO₃ and CO₂ as reaction ingredients.²¹ The CSD search also highlights the extraordinary coordinative flexibility of the CO₃²⁻ ion demonstrating bridging modes ranging from bidentate to nonadentate - with the majority (65%) being tridentate and forming M₃ triangles, a topology of inherent interest to the magnetochemist.²²

Magnetic properties

The d.c molar magnetic susceptibility, χ_M , of polycrystalline samples of complexes **1** - **5** were measured in an applied magnetic field, B , of 0.1 T, over the 2-280 K temperature, T , range. The experimental results are shown in Figure 3 in the form of $\chi_M T$ products, where $\chi = M / B$, and M is the magnetisation of the sample. At room temperature, the $\chi_M T$ product of **1** - **5** have values of 47.2, 84.1, 0.3, 8.9 and 71.3 cm³ K mol⁻¹, respectively.

These are in good agreement with the sum of Curie constants for a [Gd^{III}₆] unit (47.3 cm³ K mol⁻¹, $g_{Gd} = 2.0$) for **1**, a [Dy^{III}₆] unit (85.0 cm³ K mol⁻¹, $g_{Dy} = 4/3$) for **2**, a [Sm^{III}₆] unit (0.5 cm³ K mol⁻¹, $g_{Sm} = 2/7$) for **3**, and a [Tb^{III}₆] unit (70.9 cm³ K mol⁻¹, $g_{Tb} = 3/2$) for **5**. In the case of **4**, although the ⁷F₀ ground state of Eu^{III} possesses no magnetic moment and thus, the [Eu^{III}₆] unit should be diamagnetic at low temperatures, a finite magnetic moment is observed at room temperature, due to the low-lying ⁷F₁ first excited state that is partly populated at room temperature. Upon cooling, the $\chi_M T$ product of **1** remains essentially constant down to approximately 20 K, wherefrom it begins to decrease upon further cooling to reach 42.3 cm³ K mol⁻¹ at 2 K. Given that the anisotropy of Gd^{III} is negligible, this behaviour is consistent with the presence of weak intramolecular antiferromagnetic exchange interactions. The $\chi_M T$ product of **2** and **5** decreases continuously upon cooling, reaching 64.3 and 53.5 cm³ K mol⁻¹, respectively, at 2 K. This behaviour can be ascribed to the large magnetic anisotropy of Dy^{III} and Tb^{III} and potentially to the presence of weak intramolecular magnetic exchange interactions. The $\chi_M T$ product of **3**, remains essentially constant in the investigated temperature range, at the low, but finite, value of 0.3 cm³ K mol⁻¹, a consequence of the low Landé g -factor of the ground ⁶H_{5/2} term, indicating a splitting between the ground and first excited Kramers doublets of the ⁶H_{5/2} term larger than the thermal energy at 280 K. Finally, the $\chi_M T$ product of **4** decreases continuously upon cooling and reaches virtually zero at 2 K, reflecting the thermal depopulation of the ⁷F₁ first excited state upon cooling, likely indicating mixing of the ⁷F₀ ground state with excited states possessing a magnetic moment. To better define the low-temperature magnetic properties of complexes **1** - **5**, low temperature variable-temperature-and- variable-field (VTVB) magnetisation data were measured in the temperature and magnetic field ranges 2 to 12 K and 0 to 5 T for **1** and 2 to 8 K and 0 to 5 T for the remaining complexes. The VTVB magnetisation data of **1** are shown in Figure 3. At the highest investigated field (5 T) and the lowest investigated temperature (2 K), the magnetisation of **1** is of 42.1 μ_B (μ_B is the Bohr magneton), thus, 7.0 μ_B per Gd^{III} and in good agreement with the expected (7.0 μ_B , for $g_{Gd} = 2.0$). This observation is consistent with the presence of very weak exchange interactions operating in **1**. Furthermore, when the VTVB data of **1** are plotted against the reduced quantity $\mu_B B / kT$ (Figure S4), no nesting of the VTVB data is observed. This observation indicates that the energy spectrum of **1** does not present significant splitting with respect to the temperature of measurement at zero magnetic field. The VTVB magnetization data of **2** to **5** are shown in Figures S5 - S8, respectively. At the highest investigated field (5 T) and the lowest investigated temperature (2 K), the magnetisation of **2** and **5** is 32.0 and 29.4 μ_B , respectively, thus 5.3 and 4.9 μ_B per Dy^{III} and Tb^{III}, respectively. These values are significantly lower than the expected magnetic moment of isolated Dy^{III} (10.0 μ_B)

and Tb^{III} (9.0 μ_B) centres, for which the $m_j = -15/2$ projection of the ${}^6H_{15/2}$ ground term or the $m_j = -6$ projection of the 7F_6 ground term, respectively, is the lowest energy state. Furthermore, the VTVB data of **2** (Figure S5) and **5** (Figure S8) present nesting when plotted against $\mu_B B/kT$. These observations indicate that the energy spectrum of **2** and **5** presents significant splittings with respect to the temperature of measurement, at zero magnetic field. The VTVB magnetisation data of **3** (Figure S6) present no nesting when plotted against the reduced quantity $\mu_B B/kT$ and are also linear with magnetic field. This behaviour is consistent with the presence of a thermally isolated Kramers doublet as the ground state of the ${}^6H_{5/2}$ ground term, in agreement with the analysis of the temperature dependence of the $\chi_M T$ product. Finally, the VTVB magnetisation data of **4** (Figure S7) responds in a linear fashion with magnetic field and constant temperature, and are temperature independent at a constant field. This behaviour indicates a field-induced mixing of the 7F_0 ground state with excited states possessing a magnetic moment, consistent with the analysis of the temperature dependence of the $\chi_M T$ product.

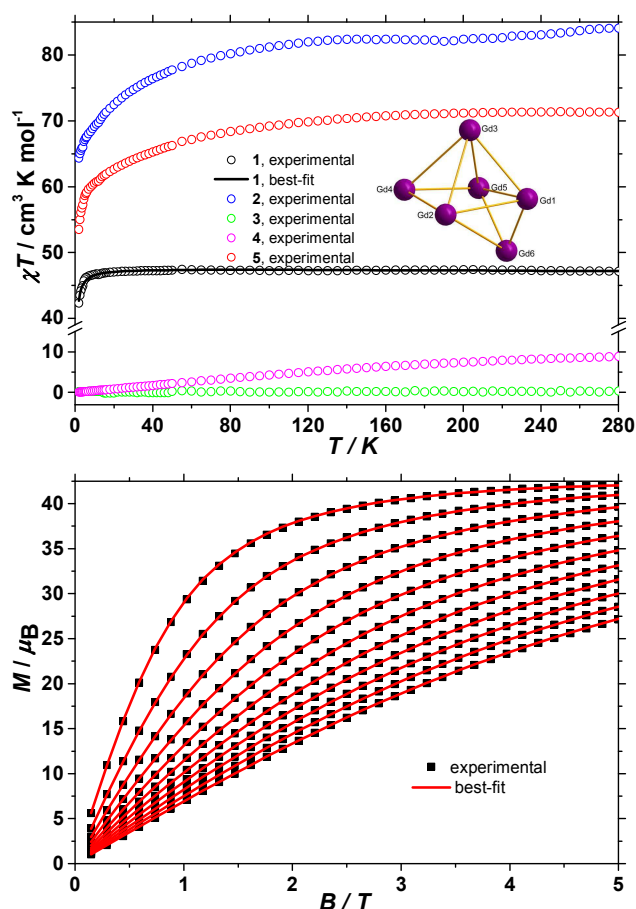


Figure 3. (Top) Temperature dependence of the $\chi_M T$ product of polycrystalline samples of **1** - **5** with $B = 0.1$ T. The inset shows the magnetic exchange pathways in the Gd₆ unit. The low-temperature field-dependence of the magnetization of **1**.

The hexanuclear nature of complexes **2** - **5**, combined with the low symmetry of the local coordination sphere of the Ln^{III} centres and the ensuing large number (twenty-seven) of associated ligand

field parameters per Ln^{III} ion, precludes any quantitative interpretation of the magnetic properties of these complexes. However, in the case of **1**, given that the orbital angular momentum for Gd^{III} is quenched, a quantitative analysis is possible through the use of a spin-Hamiltonian parameterisation. Thus, we employed the general form of the isotropic spin-Hamiltonian (1)

$$\hat{H} = \mu_B B \sum_i g_i \hat{S}_i - 2 \sum_{i,j < i} J_{ij} \hat{S}_i \cdot \hat{S}_j \quad (1)$$

where the summation indexes i, j run through the constitutive Gd^{III} centres, \hat{S} is a spin operator and J is the isotropic exchange interaction parameter. In our spin-Hamiltonian model we include the following isotropic exchange parameters: $J_{12}, J_{13}, J_{15}, J_{16}, J_{23}, J_{24}, J_{26}, J_{34}, J_{35}, J_{45}, J_{56}$ (Figure 3, top, inset) and set them all equal to J_{Gd-Gd} . Furthermore we fix $g_{Gd} = 2.0$. Thus our model contains only one free parameter, namely, J_{Gd-Gd} . The $\chi_M T$ product and VTVB data of **1** were independently fitted to spin-Hamiltonian (1) by numerical diagonalization and by use of the Levenberg-Marquardt algorithm.²³ Both fits result in the same best-fit parameter: $J_{Gd-Gd} = -0.004$ cm⁻¹. The best-fit curves are shown as solid lines in Figure 3.

Next, we report the specific heat (C) data collected for a polycrystalline sample of **1**, in the temperature range 0.3 to 30 K and in applied magnetic fields, B , of 0, 1, 3 and 7 T (Figure 4). At the higher temperatures, the specific heat is dominated by a nonmagnetic contribution arising from thermal vibrations of the lattice, which can be modelled by the Debye-Einstein model (dotted line).⁸ The phonon specific heat simplifies to a $C/R = aT^3$ dependence at the lowest temperatures, where R is the gas constant and $a = 1.1 \times 10^{-2}$ K⁻³. For $B \geq 1$ T, we model the field-dependent specific heat as the sum of the Schottky curves arising from the field-split levels of Gd^{III} independent spins (solid lines). Note the overall nice agreement with the experimental data, suggesting that applied fields of $B \geq 1$ T are nearly sufficient for fully decoupling the spin centres. The zero-applied-field specific heat can be described by the Schottky curve depicted in Figure 4 as a dashed line. This curve is calculated by assuming that every spin centre is experiencing an effective field $B_{eff} = 0.25$ T, as the result of the magnetic interactions involved. By making use of the specific heat data, we calculate the entropy (S) according to the expression $S/R = \int C/TdT$, which we plot in Figure S10 as a function of temperature and for the corresponding applied field values. The final step in the evaluation of the MCE of **1** consists in obtaining the magnetic entropy change $-\Delta S_m(T)$, for selected applied field changes ΔB . The result is shown in Figure 4. This calculation is straightforwardly obtained from the $S(T)$ curves in Figure S10 and also from the magnetisation data in Figure 3 by employing the Maxwell relation, $\Delta S_m = \int \partial M / \partial T dB$. As can be seen in Figure 4, the nice agreement between the results obtained via both methods is validation of the approaches employed. For the largest applied field change ($\Delta B = 7$ T), the magnetic entropy change, $-\Delta S_m$, reaches 22.6 J kg⁻¹ K⁻¹ at $T = 1.7$ K. Because of the very weak strength of the magnetic exchange interactions, this value of $-\Delta S_m$ is close to the maximum entropy value per mole involved, corresponding to six Gd^{III} spins ($S_{Gd} = 7/2$), calculated as $6R \ln(2 S_{Gd} + 1) = 103.7$ J mol⁻¹ K⁻¹, that is, 23.7 J kg⁻¹ K⁻¹. Thus, in **1**, nearly the full magnetocaloric potential of Gd^{III} is

achieved.

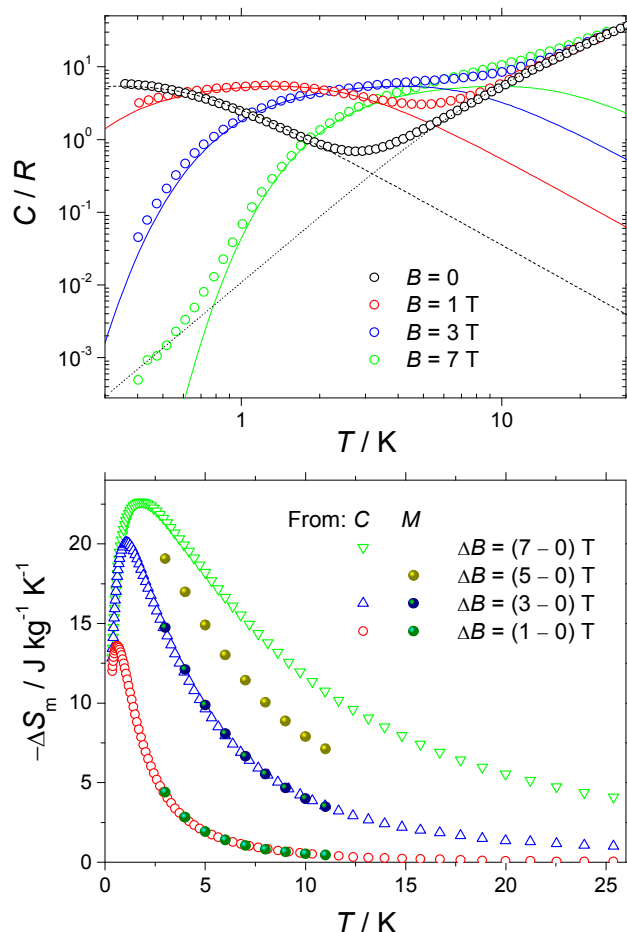


Figure 4. (Top) Molar specific heat vs. T for the labelled applied magnetic fields. Solid and dotted lines are, respectively, the Schottky and lattice contributions, calculated as explained in the text. Dashed line is the Schottky contribution, as obtained for an effective $B_{\text{eff}} = 0.25$ T. (Bottom) Temperature dependence of the magnetic entropy change for the indicated magnetic field changes. Data are obtained from specific heat (empty markers) and magnetization (full markers) experiments.

Conclusions

A highly unusual family of Ln_6Zn_2 cages whose structures are based on highly distorted bicapped octahedra can be constructed from the simple one-pot self-assembly reaction between the two metal salts and the ligand H_4L in basic methanolic solutions. The ligand has been previously used in Mn coordination chemistry to produce dodecametallic wheels and truncated tetrahedra. Magnetic exchange between the Gd^{III} ions in the octahedron is shown to be vanishingly small by independent fits of both susceptibility and magnetisation data. The MCE of complex **1** was elucidated from specific heat data, with the magnetic entropy change reaching a value of $22.6 \text{ J kg}^{-1} \text{ K}^{-1}$ at $T = 1.7$ K, close to the maximum entropy value per mole expected from six Gd^{III} spins, $23.7 \text{ J kg}^{-1} \text{ K}^{-1}$.

Acknowledgements

S.P. thanks the Danish Ministry of Science, Innovation and Higher Education for a Sapere Aude Fellowship (10-081659),

M.E. acknowledges financial support from MINECO through grant MAT2012-38318-C03-01. EKB thanks the EPSRC.

Notes and references

- ^aDepartment of Chemistry, University of Copenhagen, Universitetsparken 5, 2100, Denmark. E-mail: piligkos@kiku.dk
^bEaStCHEM School of Chemistry, The University of Edinburgh, David Brewster Road, Edinburgh, Scotland, EH9 3FJ, UK. E-mail: ebrechin@staffmail.ed.ac.uk
^cInstituto de Ciencia de Materiales de Aragón and Departamento de Física de la Materia Condensada, CSIC-Universidad de Zaragoza, 50009 Zaragoza, Spain. E-mail: evange@unizar.es
- † Electronic Supplementary Information (ESI) available: crystallographic data in tabulated format, and additional structural and magnetic figures.
- J. D. Rinehart and J. R. Long, *Chem. Sci.*, 2011, **2**, 2078.
 - D. N. Woodruff, R. E. P. Winpenny and R. A. Layfield, *Chem. Rev.*, 2013, **113**, 5110.
 - R. Sessoli and A. K. Powell, *Coord. Chem. Rev.*, 2009, **253**, 2328.
 - L. Sorace, C. Benelli and D. Gatteschi, *Chem. Soc. Rev.*, 2011, **40**, 3092.
 - Lanthanides and Actinides in Molecular Magnetism*, Eds., R. A. Layfield and M. Murugesu, Wiley VCH, 2015.
 - E. K. Brechin and G. Aromí, *Struct. Bond.*, 2006, **1**, 1; C. J. Milios and R. E. P. Winpenny, *Struct. Bond.*, 2015, **164**, 1.
 - M. Evangelisti in *Molecular Magnets, NanoScience and Technology*, Eds., J. Bartolomé, F. Luis, J. F. Fernández, Springer, Berlin, 2014, pp. 365-387.
 - M. Evangelisti, F. Luis, L. J. de Jongh and M. Affronte, *J. Mat. Chem.*, 2006, **16**, 2534.
 - M. Evangelisti and E. K. Brechin, *Dalton Trans.*, 2010, **39**, 4672.
 - J. W. Sharples and D. Collison, *Polyhedron*, 2013, **54**, 91.
 - M. Evangelisti, A. Candini, A. Ghirri, M. Affronte, E. K. Brechin and E. J. L. McInnes, *Appl. Phys. Lett.*, 2005, **87**, 072504; R. Shaw, R. H. Laye, L. F. Jones, D. M. Low, C. Talbot-Eckelaers, Q. Wei, C. J. Milios, S. Teat, M. Helliwell, J. Raftery, M. Evangelisti, M. Affronte, D. Collison, E. K. Brechin and E. J. L. McInnes, *Inorg. Chem.*, 2007, **46**, 4968.
 - M. Manoli, R. D. L. Johnstone, S. Parsons, M. Murrie, M. Affronte, M. Evangelisti and E. K. Brechin, *Angew. Chem., Int. Ed.*, 2007, **46**, 4456; M. Manoli, A. Collins, S. Parsons, A. Candini, M. Evangelisti and E. K. Brechin, *J. Am. Chem. Soc.*, 2008, **130**, 11129.
 - G. Karotsis, M. Evangelisti, S. J. Dalgarno and E. K. Brechin, *Angew. Chem., Int. Ed.*, 2009, **48**, 9928; G. Karotsis, S. Kennedy, S. J. Teat, C. M. Beavers, D. A. Fowler, J. J. Morales, M. Evangelisti, S. J. Dalgarno and E. K. Brechin, *J. Am. Chem. Soc.*, 2010, **132**, 12983.
 - K. S. Pedersen, G. Lorusso, J. J. Morales, T. Weyhermüller, S. Piligkos, S. K. Singh, D. Larsen, M. Schau-Magnussen, G. Rajaraman, M. Evangelisti and J. Bendix, *Angew. Chem., Int. Ed.*, 2014, **53**, 2394.
 - M. Evangelisti, O. Roubeau, E. Palacios, A. Camón, T. N. Hooper, E. K. Brechin and J. J. Alonso, *Angew. Chem. Int. Ed.*, 2011, **50**, 6606.
 - S. K. Langley, N. F. Chilton, B. Moubaraki, T. Hooper, E. K. Brechin, M. Evangelisti and K. S. Murray, *Chem. Sci.*, 2011, **2**, 1166.
 - J. W. Sharples, D. Collison, E. J. L. McInnes, J. Schnack, E. Palacios, and M. Evangelisti, *Nature Comm.*, 2014, **5**, 5321; J. W. Sharples, Y.-Z. Zheng, F. Tuna, E. J. L. McInnes and D. Collison, *Chem. Commun.*, 2011, **47**, 7650.
 - G. Lorusso, J. W. Sharples, E. Palacios, O. Roubeau, E. K. Brechin, R. Sessoli, A. Rossin, F. Tuna, E. J. L. McInnes, D. Collison and M. Evangelisti, *Adv. Mater.*, 2013, **25**, 4653.
 - S. Sanz, J. M. Frost, M. B. Pitak, S. J. Coles, S. Piligkos, P. J. Lusby and E. K. Brechin, *Chem. Commun.*, 2014, **50**, 3310; J. M. Frost, S. Sanz, T. Rajeshkumar, M. B. Pitak, S. J. Coles, G. Rajaraman, W. Wernsdorfer, J. Schnack, P. J. Lusby and E. K. Brechin, *Dalton Trans.*, 2014, **43**, 10690.

-
- 20 See for example: J. B. Peng, Q. C. Zhang, X. J. Kong, Y. Z. Zheng, Y. P. Ren, L. S. Long, R. B. Huang, L. S. Zheng and Z. Zheng, *J. Am. Chem. Soc.*, 2012, **134**, 3314.
- 21 See for example: Y. N. Guo, X. H. Chen, S. Xue and J. Tang, *Inorg. Chem.*, 2012, **51**, 4035; T. N. Hooper, R. Inglis, M. A. Palacios, G. S. Nichol, M. B. Pitak, S. J. Coles, G. Lorusso, M. Evangelisti and E. K. Brechin, *Chem. Commun.*, 2014, **50**, 3498.
- 22 J. Schnack, *Dalton Trans.*, 2010, 39, 4677.
- 23 W. H. Press, S. A. Teukolsky, W. T. Vetterling, B. P. Flannery,
10 *Numerical recipes in C: The Art of Scientific Computing*, 2nd ed., Cambridge University Press, Cambridge, 1992.